Key Engineering Materials
ISSN: 1662-9795, Vol. 932, pp 77-101

Submitted: 2022-01-02
Revised: 2022-02-19
Accepted: 2022-02-23
Online: 2022-09-20

Characterizing Groundwater Turbidity Reduction by Using a Magnetic Biocarbon Adsorbent Composite (MBAC): Process Optimization

Huda Awang[1a], Nor Asfaliza Abdullah[1b], Ho Yoon Ling[1c], Irene Tan Jia Lin[1d], Palsan Sannasi Abdullah[1e*], Siti Nuurul Huda Mohammad Azmin[1f] and Fatima Boukhlifi[2g]

[1]Faculty of Agro Based Industry, Universiti Malaysia Kelantan Jeli Campus, 17600 Jeli, Kelantan, Malaysia

[2]Faculty of Sciences, Moulay Ismail University, BP 11, 201-Zitoune, Meknes, Morocco

[a]hudaawang@gmail.com, [b]asfalizaabdullah@gmail.com, [c]yoonling_96@gmail.com, [d]jialinirene95@gmail.com, [e]palsan.abdullah@umk.edu.my, [f]huda.ma@umk.edu.my, [g]f.boukhlifi@umi.ac.ma

Keywords: activated carbon; factorial design; iodine number; response surface methodology; turbidity.

Abstract. The use of groundwater as drinking water source in many parts of Kelantan encourages the research and development of various cost-effective alternative adsorbent material for turbidity reduction and drinking water purification. The preparation, characterization, and use of a magnetic biocarbon adsorbent composite (MBAC) is introduced in this study as an option to treat turbid groundwater. In contrast to commercial activated carbon (CAC), peak shifts and peaks denoting Fe-O bending were observed in the FTIR spectrum of MBAC. The adsorption process for turbidity reduction by MBAC and CAC was investigated. A factorial design matrix consisting of four parameters were tabulated, namely, adsorbent dosage (0.02, 0.04, and 0.06 g), agitation time (15, 30, and 60 min), agitation rate (150, 200, and 250 rpm), and two adsorbent particle size ranges (M: $300 < x \leq 500$ μm, and Q: ≤ 45 μm). The predictive model was validated with 0.04 g MBAC of $\leq$ 45 μm in particle size, agitated at 150 rpm, for 48 min, that attained 98.46% turbidity removal efficiency with a final NTU reading of 0.40. Conversely, CAC removed 88.19% for a final NTU reading of 3.07. Overall, the iron oxide impregnated biocarbon composite showed better turbidity reduction capability compared to CAC. The findings of this work support the potential application of MBAC as an alternative adsorbent for the treatment of groundwater sourced drinking water.

Introduction

The use of groundwater for daily water needs is common in many parts of the state. It has been reported that in Kelantan, the average water production in 2020 was 503 million L per day, of which 60% was sourced from groundwater; and over half of the population uses groundwater for daily consumption. Air Kelantan Sdn. Bhd. (AKSB) has been recognised as the largest groundwater operator in Malaysia, up to 180.6 million L water per day [1]. The state water service provider derives the 84.25% of water for domestic and industrial demand from groundwater treated at their water treatment plants. In contrast to treated water supplied by water service providers to consumers, less attention is given to groundwater treatment at point of source and at point of use. In addition, poor conditions of supply pipes further deteriorate the receiving water quality. Furthermore, about 38% of the population in Kelantan use alternative means of obtaining groundwater directly through wells, tube wells, and bored wells without adequate prior treatment for their daily consumption. This is because water supply service coverage in Kelantan stands at 76.2% for rural areas and 62.4% for urban areas as opposed to Peninsula's overall coverage of > 96% [2]. This calls for research and development into various cost-effective alternative adsorbent material for turbidity reduction and drinking water purification. Rapid growth of population and accelerated urbanization further increases groundwater consumption.

Groundwater can be contaminated through surface and subsurface water infiltration, also from substances released through anthropogenic activities or natural causes. Flooding as encountered in Kelantan during the monsoon season causes increase in suspended solids and its subsequent flow into groundwater. The material spread is governed by diffusion, dispersion, and adsorption. Contamination of groundwater can result in poor drinking water quality and water supply disruption.

Furthermore, inadequate waste management, excavation of land above or near the aquifer may lead to turbid groundwater [3]. Turbidity formation and water fouling are due to the decomposition or decaying of organic matter by soil microorganisms known as humus, and the presence of peat soil with high iron content [4]. Turbid groundwater not only reduces the aesthetic quality of the water but is also associated with gastrointestinal acid reflux disease among consumers [5]. It is important to remove undesirable odour, taste, colour and other components from the water. One of the main parameters set as water quality indicator is turbidity [2]. Turbidity is measured in nephelometric turbidity units (NTU). The turbidity standard for drinking water is 5 NTU or less [6, 7].

In conventional water treatment, many chemicals and inorganic coagulants are applied for clarifying water and to reduce turbidity. Among others, aluminium chlorohydrate (ACH), polyaluminum chloride (PAC), and alum (Al_2SO_4) which can pose negative effects towards health [8]. As for water treatment, *ex situ* groundwater remediation approaches include photocatalytic, chemical precipitation (hydrolysis), and coagulation. Adsorption is one of the more preferred conventional clean-up methods for water treatment practiced by water solution providers, and industries alike. This is due to simplicity in its process and better performance. But these processes are impractical to be applied at every household's point of use.

Activated carbon (AC) is the widely used adsorbent as it displays high adsorption capacity and able to remove a broad range of contaminants such as organic pollutants and heavy metals [9]. The recovery of spent material through gravitational separation can be challenging due to small particle size, therefore increasing the costs for additional treatment [10]. The spent chemicals can lead to secondary pollution issues due to sludge generation. Apart from that, filtration is less practical for treatment of large volume of streams such as groundwater, and may display lower sorptive capacity and ability, require pre and post treatment routines, and overall treatment cost increase [11].

Recently, the use of iron oxide-based magnetic nanomaterials had been proposed as an alternative adsorbent with higher adsorption, higher surface-area-to-volume ratio, surface modifiability capability, excellent magnetic properties, ease of separation, lower operation costs, and environmentally friendly, among others [11,12]. But free iron oxide magnetic particles in the form of hematite (α-Fe_2O_3), magnetite (Fe_3O_4), and maghemite (γ-Fe_2O_3) are prone to self-aggregation in solution and need to undergo surface modification to be anchored onto an organic molecule to overcome the issue [13].

Magnetic activated carbon (MAC) can be defined as a class of porous carbon-rich material that offers high surface area coupled with magnetic property for increased adsorption capability and efficiency [14]. Activated carbon are usually produced through activation with steam at very high temperatures of up to 1100 ºC-1200 ºC. This is in contrast to biocarbon which can be defined as carbon-rich, porous substance, which can be produced by thermal decomposition of biomass through carbonization under air-limited enclosed conditions and at relatively lower temperatures.

In this paper, we describe our attempt in developing an adsorbent composite composed of iron oxide impregnated coconut shell biocarbon for potential use in turbidity reduction of local groundwater sourced from a well in Tanah Merah area. The interactive factors for process optimization (i.e., adsorbent dosage, particle size range, agitation rate, and agitation time) were tabulated and identified. The findings from this study are hoped to help the development of a magnetic biocarbon adsorbent composite (MBAC) based filter system at the point of use. This can then be presented in an all-in-one water filtration system at the point of use areas rather than having separate methods to address coagulation, flocculation, and membrane filtration [15].

Materials and Methods

Materials (chemicals and reagents). The following materials were used; ammonium hydroxide (NH_4OH, 0.7 M; R&M), iron (III) chloride hexahydrate ($FeCl_3.6H_2O$; R&M), iron (II) sulphate heptahydrate ($FeSO_4.7H_2O$; R&M), iodine pearl (Friendemann Schmidt), potassium iodide (KI; Friendemann Schmidt), sodium thiosulphate pentahydrate ($Na_2S_2O_3.5H_2O$; Friendemann Schmidt), sodium carbonate (Na_2CO_3; R&M), methylene blue (Bendosen), epichlorohydrin (C_3H_5ClO; Merck), ethanol 95% AR grade, 10% (w/v) starch solution, potassium hydroxide (KOH; HmbG), sodium hydroxide (NaOH; HmbG), hydrochloric acid (HCl; HmbG), commercial activated carbon (CAC; Ki Carbon), neodymium (NdFeB) N52 magnet.

Preparation of magnetic biocarbon adsorbent composite (MBAC). The magnetic biocarbon adsorbent composite (MBAC) is a combination of coconut shell (CS) derived activated biocarbon (ABC) impregnated with iron oxide particles. The coconut shells were carbonized in a 200 L modified carbonization drum through top lit up-draft (TLUD) approach [16]. The carbonized CS (CCS) pieces were washed, left to dry, then crushed into powder form, and sieved (Auto sieve shaker, Model: A060-01) before segregated into 5 particle size ranges (M: $300 < x \leq 500$; N: $150 < x \leq 300$; O: $75 < x \leq 150$; P: $45 < x \leq 75$; and Q: ≤ 45). For the purpose of this work, only portion M and Q were utilized. The CCS was subjected to base activation using KOH as described by Nor Asfaliza et al., [17] to yield CSABC. A revised chemical co-precipitation method was followed, where the CSABC was soaked with 6 M HCl for 4 h at 40-50 ºC, and later oven dried at 80 ºC [18]. An aqueous mixture was made by dissolving 19.5 g $FeCl_3.6H_2O$ and 10.0 g $FeSO_4.7H_2O$ in 450 mL of distilled water. The solution was heated to 70 ºC, and NH_4OH was added gradually (~50 mL) while monitoring the pH to not exceed pH 10-10.5. Then, the temperature was increased to 85 ºC while adding 15 g of CSABC (3% w/v) and mixed well. This was followed by addition of C_3H_5ClO (6 mL), agitation for 1 h, and sonication (QSonica Q500) for another 1 h. Finally, the solid mixture was left to cool down to room temperature, washed, rinsed rapidly with water-ethanol solution mix until pH dropped to pH 6.5-7, before collected with neodymium (NdFeB) N52 magnet, and oven dried (80 ºC). The MBAC powder was stored in an air-tight container prior to use.

Iodine number (IN) determination. The following solutions were prepared and procedures followed as outlined in ASTM D4607-94 [19]. (i) A 0.05 N $Na_2S_2O_3$ solution was prepared by dissolving 12.40 g of $Na_2S_2O_3$ in approximately 75 ± 25 mL of boiled distilled water. A 0.10 ± 0.01 g of Na_2CO_3 was added into the solution to reduce acidity and minimize decomposition. The mixture was then transferred into a 1 L volumetric flask and diluted with distilled water until the mark. The solution was stored in an amber bottle and left to stand for 4 days before standardization. (ii) A standard 0.1 N of iodine solution was prepared by mixing 12.70 g of iodine pearls and 19.10 g of potassium iodide (KI) with 2 to 5 mL of distilled water. Small volume (about 5 mL) of distilled water was continuously added each time into the beaker until the total volume of the solution reached 50 mL. The solution was left to stand (about 4 h) with occasional stirring to ensure the crystals were completely dissolved. The solution was transferred into a 1 L volumetric flask, filled with distilled water until it reached the mark and stored in an amber bottle. (iii) Starch solution was prepared by dissolving 1.0 ± 0.5 g of starch in 5 to 10 mL of cold water. Then, 25 ± 5 mL of distilled water was added while stirring. The starch paste was poured into 1 L of boiling water and boiled for 4 to 5 min.

Firstly, 10 mL of iodine solution was titrated with 0.05 N $Na_2S_2O_3$ until the solution turned to pale yellow, then 2 drops of starch solution was added, and titration continued until the solution became colourless. This was recorded as the blank volume reading (B, mL). Next, about 0.2 g of MBAC was introduced into a flask containing 40 mL of 0.1 N iodine solution and agitated for 50 min at 200 rpm (orbital shaker; WSZ-100A). The MBAC was separated from the solution by using the N52 magnet. The residual solution (10 mL) was titrated against 0.1 N $Na_2S_2O_3$ solution as before, until the solution turned colourless. The $Na_2S_2O_3$ volume consumed with the sample was noted (A, mL). The consumed volume difference between blank (B, mL) and sample (A, mL), was

read as C (mL) = B – A. All runs were performed in triplicates, and the mean values recorded. The conversion factor (C.F.) was determined as in Eq. 1, and the iodine number (IN) was expressed in mg/g and calculated as in Eq. 2 [20, 21]:

$$\text{Conversion factor (C.F.)} = \frac{\text{IMM} \times \text{NI} \times \text{VI}}{\text{w} \times \text{B}} \quad (1)$$

$$\text{Iodine number, IN (mg/g)} = \text{C (mL)} \times \text{C.F.} \quad (2)$$

Where, IMM is the iodine molar mass (126.92 g/mol), NI is the normality of iodine (N), VI is the volume of iodine solution (40 mL), w is the weight of adsorbent (g), and B is the blank volume of $Na_2S_2O_3$ (mL).

Characterization of CAC and MBAC. Proximate analysis was carried out to determine volatile matter, moisture, ash, and fixed carbon content as per procedure described by Milne et al., [22]. The surface area by IN estimation (SA_{calc}) was calculated using Eq. 3, where IN (from Eq. 2) is the iodine number (mg/g), N_A is the Avogadro constant = 6.02 x 10^{23}/mol, and ω is the iodine surface area = 2.096 x 10^{-19} m^2 [2]:

$$SA_{calc} = [IN \times 10^{-3} \times N_A \times \omega] / IMM \quad (3)$$

The experimental Brunauer Emmett Teller (BET) surface area (m^2/g), total pore volume (cm^3/g), average pore diameter (nm), and pore size were obtained through BET analysis of N_2 adsorption desorption isotherm at 77K (Quantachrome Autosorb iQ3 Automated Gas Sorption Analyzer). The N_2 adsorption isotherm was used to estimate the pore volume at relative pressure of 0.98 [21]. Fourier transform infrared (FTIR, ATR) spectroscopy (Thermo Scientific Nicolet iN10 Infrared Microscope & iZ10 FTIR module) was performed in the 500-4000 cm^{-1} range to screen the functional groups in both adsorbents. Surface morphology was visualized through scanning electron microscopy (SEM) coupled to energy dispersive spectroscopy (EDS) (JEOL Model JSM IT100) with an acquisition time of 40 s and accelerating voltage of 15-20 kV.

Water sampling and turbidity measurement. The groundwater was obtained from a well (designated as S2) in Tanah Merah, Kelantan (GPS coordinate: 5°49'31.7"N, 102°07'36.2"E; 5.825472, 102.126722). The initial turbidity reading of this raw groundwater was approximately in the range of 20-32 NTU. Turbidity was measured using turbidity meter with fast tracker (HI98703 Turbidity Portable Meter, Hanna Instruments, Romania).

Turbidity reduction studies via Response Surface Methodology (RSM) approach. The turbidity reduction studies were conducted by batch method with 10% (w/v) adsorbent in the working volume. In order to study the turbidity reduction and removal efficiency responses to variation in parameters, the 3-factorial experimental design through Response Surface Methodology (RSM) approach was opted (Table 1). The numerical factors consisted of adsorbent dosage, agitation time, and agitation rate, denoted as A, B, and C, respectively. Meanwhile the categorical factor was adsorbent particle size range, coded as D. This was done as in reality and in practice, adsorbents cannot be exclusively separated to one single fixed size. The levels of each factor were coded as -1 (low), 0 (middle), and 1 (high) as in Table 1.

Table 1. Experimental design and the factor levels

Factor types	Factors	Unit	Code	Levels		
				-1	0	1
Numerical	Adsorbent dosage	g	A	0.02	0.04	0.06
	Agitation time	min	B	15	30	60
	Agitation rate	rpm	C	150	200	250
Categorical	Adsorbent particle size range	μm	D	≤ 45		300 < x ≤ 500

A commercial activated carbon (CAC) sample was included for process comparison with MBAC. Turbidity reduction was reported as turbidity removal percentage (%), Eq. 4, where C_i and C_f are initial and final nephelometric turbidity units (NTU) reading, respectively.

$$\text{Turbidity Removal (\%)} = \frac{C_i - C_f}{C_i} \times 100 \quad (4)$$

Results and Discussions

Characterization of MBAC and CAC. The preparation of MBAC through modified chemical co-precipitation was successful and the solid composite can be easily separated from any aqueous solution by aid of a magnet or external magnetic field (Fig. 1). The main difference between the two adsorbents is the magnetic property of MBAC. There are various techniques to prepare magnetic Fe_3O_4 or magnetic biochars, among them are chemical co-precipitation, microwave heating, hydrothermal synthesis, thermal decomposition, and micro-emulsion [23]. In this work, the preparation procedure of MBAC did not require vigorous stirring of the solution mix in the presence of N_2 or CO_2 gas. The stability of the newly prepared iron impregnated adsorbent was tested by mixing the composite in water (10%, w/v), agitated daily for 30 d. No trace of iron leaching was detected (iron checker, Hanna HI 721).

Fig. 1. The response of MBAC to the presence of an external magnetic field. The feature ease separation of adsorbents dispersed in liquid sample. The redispersion-separation cycle can be repeated

Proximate analysis. The results of proximate analyses (Table 2) shows that MBAC possesses higher moisture, ash, pH, and apparent density compared to CAC.

Table 2. Characterization properties of MBAC and CAC

Parameter		MBAC	CAC
Moisture content (%)		6.70	4.37
Ash content (%)		19.23	5.71
Volatile (%)		12.52	15.40
Fixed carbon (%)		66.50	79.95
pH		7.8	6.6
Apparent density (g/cm^3)		0.552	0.305
Lead, Pb (ppm)		n.d.	n.d.
Iodine number (mg/g)	≤ 45 μm	925.84	1305.16
	300 < x ≤ 500 μm	724.19	1007.00
BET surface area (S_{BET}, m^2/g)	≤ 45 μm	916.19	1084.07
	300 < x ≤ 500 μm	309.35	769.50
Surface area calculated (SA_{calc}, m^2/g)	≤ 45 μm	920.44	1297.54
	300 < x ≤ 500 μm	719.96	1001.12
Pore volume (cm^3/g)	≤ 45 μm	0.668	0.662
	300 < x ≤ 500 μm	0.303	0.460
Average pore diameter (nm)	≤ 45 μm	14.6	18.57
	300 < x ≤ 500 μm	20.24	20.53

The moisture content of MBAC was higher than CAC by 3.7% and is likely because of the moisture adsorbing nature of the composite, and the iron oxide nanoparticles found in MBAC pores [24]. MBAC had higher ash content (19.23%), which was 70% more compared to CAC. Ash are incombustible mineral residues such as calcium, magnesium, iron, sodium, phosphorus, and potassium which are present in the pores of the biomass [25]. This can be attributed to the impregnation of MBAC with iron oxides. Zhao et al., [26] reported a higher ash content of 28.48% in magnesium added palm kernel biochar composite, Mg-PKS. Apparent density reflects the weight of carbon per unit volume. MBAC was also denser than CAC by 44% due to the presence of additional iron element. Higher density denotes better quality as there is more available volume. The volatile matter and fixed carbon range of both MBAC and CAC were comparable to those reported by Hidayu et al., [27] for activated carbon of oil palm empty fruit bunch (EFB), which was 15.23% and 67.66%, respectively. CAC displayed higher fixed carbon value (79.95%) than MBAC (66.50%).

IN determination, BET surface area, and pore properties. Iodine number (IN, mg/g) which describes iodine adsorption is an important parameter that reflects the presence of micropores (up to 20Å or 2 nm) and provides a rough estimate of total surface area. Higher fixed carbon supports increased pore structure forming. This explains the higher iodine number (1007-1305.16 mg/g) and BET surface area (769.50-1084.07 m^2/g) with both particle size ranges of CAC. Generally, with both adsorbents, the smaller sized particle (i.e., ≤ 45 μm) presented higher IN, and surface area reading than particles in the 300 < x ≤ 500 μm range. As seen from Table 2, MBAC showed lower IN (724.19-925.84 mg/g) as opposed to CAC (1007.00-1305.16 mg/g). Higher iodine number indicates higher degree of activation. The impregnation with iron oxides had caused a decrease in its effective surface area and micropore volume thus explaining the lower IN and BET surface area. The lower surface area of MBAC in contrast to CAC is likely due to pore block from covering and layering of iron oxide particles arising from the magnetization process. This was more evident with larger sized MBAC (300 < x ≤ 500 μm) which had lower BET surface area of 309.35 m^2/g, while CAC's surface area was more than double at 769.50 m^2/g. Pore volume space were adequate with both adsorbents, without any significant difference between them. These suggests that even though lower surface area was observed with MBAC, the carbano-magnetization process of iron oxide impregnation did not affect porosity of the adsorbent when compared to CAC. Anyika et al., [34] reported a higher specific surface area (1225 m^2/g), total pore volume (0.2943 cm^3/g), and lower average pore diameter (2.05 nm) for palm kernel shell activated carbon (PKSAC) when compared

to another CAC (surface area = 846.15 m^2/g), magnetic CAC (surface area = 833.73 m^2/g), and palm kernel shell treated with ferric chloride and ferrous sulphate (surface area = 257.86 m^2/g; total pore volume = 0.1124 cm^3/g, average pore diameter = 3.39 nm). Surface property readings differed when compared to bare Fe_3O_4 nanoparticles which experienced agglomeration and displayed lower surface area (93.67 m^2/g), pore volume (0.29 cm^3/g), and average pore diameter (12.34 nm) as described by Wan Fatihah et al., [23]. The activated carbon prepared from oil palm empty fruit bunch (EFB) on the other hand had a BET surface area of 720 m^2/g, total pore volume of 0.341 cm^3/g with average pore diameter of 1.90 nm [27]. Thus, surface properties greatly vary between adsorbent material governed by precursor type, modifications performed, preparation procedure and conditions. The typical range of IN for adsorbents or activated carbons used in water and wastewater application is around 500-1200 mg/g [28]. Hence, MBAC is comparatively suitable as an adsorbent in terms of surface area and porosity [29], with an added feature of magnetism.

FTIR analysis. The spectra of CAC and MBAC are shown in Fig. 2. For better comparison, the plots can be grouped into 6 areas which falls within the following wavelength (cm^{-1}) range: 500-550, 550-1300, 1300-1900, 1900-2400, 2400-3400, and 3400-4000. The peak signatures in the 1300-4000 cm^{-1} range were quite identical reflecting common nature of biomass origin, that only differed in their intensity. Among the common functional groups were alkanes with strong C-H stretching (2850-3000 cm^{-1}), and the flat peaks in the 3600-3800 cm^{-1} range represented hydroxyl (OH) groups [30, 31]. The flat or absence of peaks at 2900-2980 cm^{-1} (of C-H stretching) indicated complete carbonization [32].

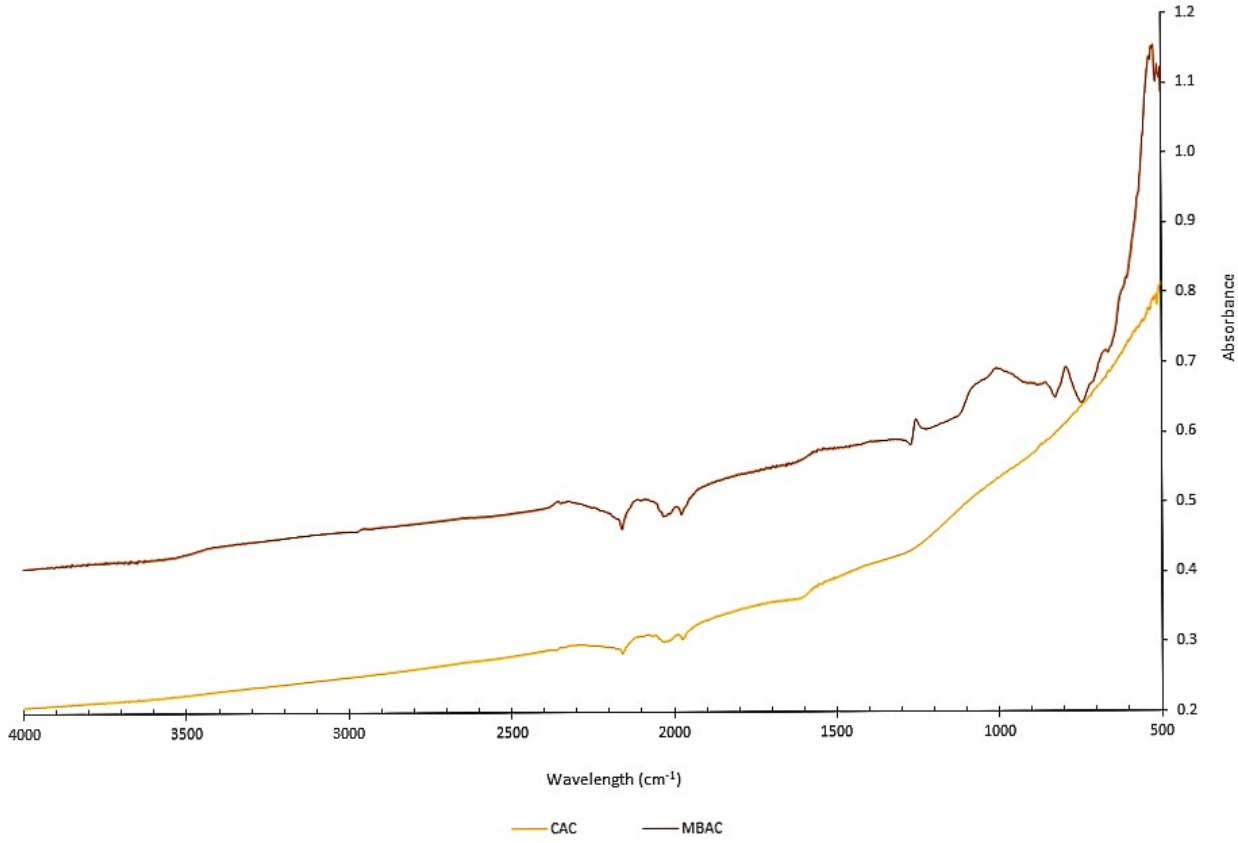

Fig. 2. FTIR spectra of CAC and MBAC. For comparison, the plot scan be grouped into 6 areas within the following wavelength (cm^{-1}) range: 500-550, 550-1300, 1300-1900, 1900-2400, 2400-3400, and 3400-4000

In addition, the humps in the 1900-2250 cm^{-1} range were due to alkenes with strong C=C asymmetric stretch (1900-2000 cm^{-1}), C≡C (of aromatic compounds), and medium C=C=C stretching from hydrocarbon residues. Medium stretch vibrations of -N=C=O, -N=C=S, -N=C=N, and C=C=O can be observed at 2100-2270 cm^{-1} [30,31]. The C=O stretch lies in the narrow 1510-1700 cm^{-1} range. The broad line in the 1600-1750 cm^{-1} range denotes weak C-H bending, medium C=C stretching, and medium C=N stretching of aromatic compounds, alkene and imine groups. Significant peaks and positioning differences between CAC and MBAC are seen over the 500-550 cm^{-1} and 550-1300 cm^{-1} group block range. With regards to MBAC, the new peaks at 522-530 cm^{-1} range correspond to Fe-O stretch. Metal oxygens stretches are usually observed below 1000 cm^{-1}. Wan Fatihah et al., [23] described Fe-O bond vibration in the range of 579-635 cm^{-1}, Mirzaei et al., [32] reported of Fe-O deformation at 560 cm^{-1}, and Lin et al., (2015) noted of Fe-O stretching at 523-537 cm^{-1}. Similarly, Anyika et al., [34] observed peaks of Fe_3O_4 at 529 cm^{-1} and 616 cm^{-1} with a magnetic palm kernel shell sample. The noticeable variation within the 550-1300 cm^{-1} denoted strong to medium alteration in C=C bending of alkene functional groups, strong bending of C-H deformation (600-700 cm^{-1}), medium to strong in-plane C=H bending (690-900 cm^{-1}), and strong bending vibrations of =C-H and CH_2 (880-995 cm^{-1}). This would be due to the carbano-magnetization process carried out during the preparation of MBAC which dealt with surface modification of the biocarbon. No peaks were observed for CAC in the similar area range. The CAC spectrum was identical to that reported by Hidayu et al., [27].

Surface characterization. Fig. 3 depicts SEM images and EDAX plots of CAC and MBAC. The intense pore-built structure of C rich CAC was clearly visible, which explains the higher IN and BET surface area value readings. The form of MBAC differed in terms of pore uniformity and its composition due to the presence of Fe. The agglomeration and coverage of iron oxides over the biocarbon pores may have contributed to the lower IN and surface area. The iron oxides may induce pore blockage as noted by Suresh Kumar et al., [33]. Similar micrographs of scattered iron oxide deposits were seen with magnetic palm kernel shell as reported by Anyika et al., [34]. Elemental (atomic %) composition summary revealed the main variation between the two adsorbents. CAC has higher C content (90.24%) and void of iron (Fe). MBAC on the other hand, showed the presence of Fe (33.48%), attributed to the iron oxide in addition to C (28.63%) and O (37.89%). This result concurs with the FTIR observation for the presence of Fe-O stretch in MBAC. Anyika et al., [34] had described of a magnetic palm kernel shell which contained C (32.83%), O (45.48%), Fe (20.37%), and P (1.32%). The crystallinity features of the iron deposits had been characterized by X-ray diffraction (data reported elsewhere), and were found to be composed mainly of γ-Fe_2O_3 (maghemite), Fe_3O_4 (magnetite), and FeO (wuestite). The presence of iron oxide particles give rise to the ferromagnetic property of MBAC and are superparamagnetic in behaviour [35]. This will produce greater affinity towards multi adsorbates adsorption and enables easier after use separation of spent adsorbent material.

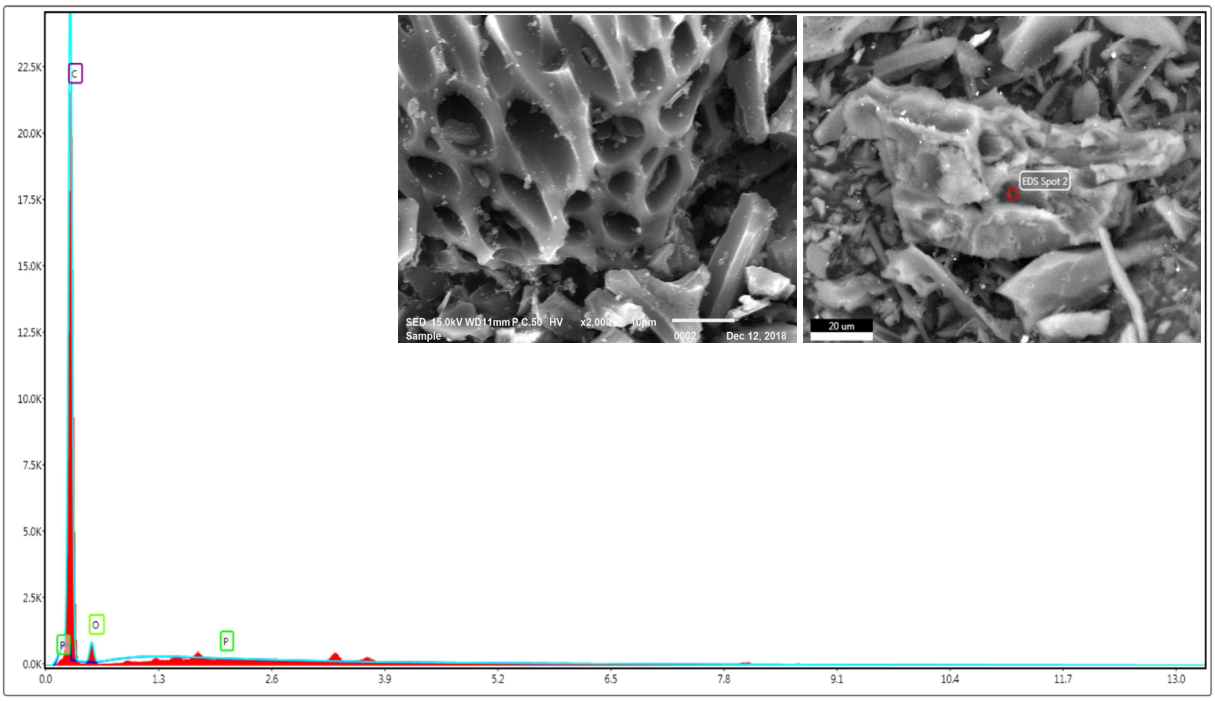

(a)

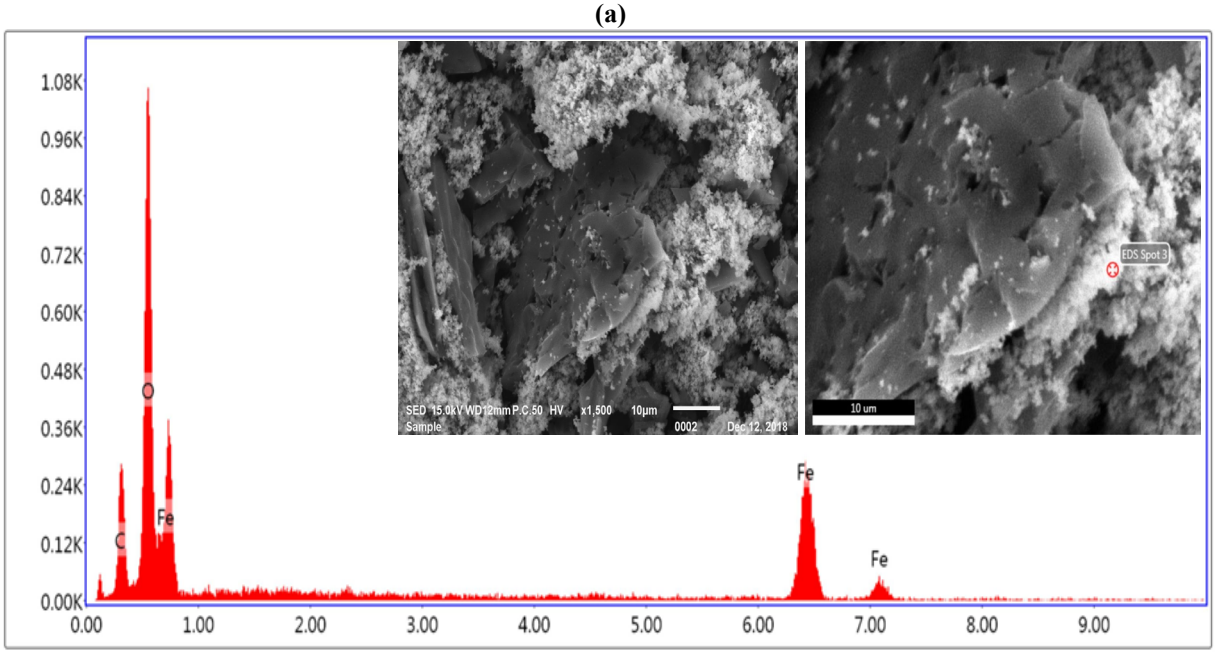

(b)

Fig. 3. Surface characterization through SEM and EDAX, **(a)** plot of CAC showing elemental peaks and atomic % attributed to C (90.24%), O (9.76%), and P (0.01%) clearly indicating the impregnation of iron oxides in the biocarbon composite; **(b)** plot of MBAC showing elemental peaks and atomic % attributed to C (28.63%), O (37.89%), and Fe (33.48%) clearly indicating the impregnation of iron oxides in the biocarbon composite. Data captured through eZAF Smart Quant (kV: 15-20, Mag: 1000-3300, Take off: 37.8-40.7, Live time (s): 30, Amp time (µs): 1.92, Resolution: (eV): 128.9

Turbidity reduction study. The design matrix (codified value) encompassing of the important parameters that affect process optimization and the corresponding response value, i.e., turbidity removal efficiency % are shown in Table 3. Overall, both adsorbents (MBAC and CAC) are useful and able to reduce turbidity of raw groundwater. It was observed that MBAC displayed greater turbidity removal, in the higher range of 84%-98%, while CAC fell within 65%-92%.

Table 3. Decodified variables (A, B, C, and D) and turbidity removal (%) response for MBAC and CAC

Run	Coded variables				Response	
	A: Dosage of adsorbent	B: Time of agitation	C: Agitation rate	D: Size of adsorbent	Removal Efficiency (%)	
	g	min	rpm	um	MBAC	CAC
1	0.02	15	150	≤ 45	93.69	83.77
2	0.02	30	250	≤ 45	93.84	79.93
3	0.04	15	200	≤ 45	94.33	74.29
4	0.06	15	250	≤ 45	96.33	80.65
5	0.02	60	200	≤ 45	96.93	64.25
6	0.04	30	150	≤ 45	97.94	87.6
7	0.04	60	250	≤ 45	97.04	82.47
8	0.06	30	200	≤ 45	95.37	73.24
9	0.06	60	150	≤ 45	98.51	89.80
10	0.04	30	200	≤ 45	97.22	78.29
11	0.04	30	200	≤ 45	96.34	78.04
12	0.06	15	150	≤ 45	92.53	77.84
13	0.06	30	250	≤ 45	97.98	83.78
14	0.02	15	200	≤ 45	94.89	79.86
15	0.04	15	250	≤ 45	97.93	86.42
16	0.02	15	150	300 < x ≤ 500	85.75	87.31
17	0.02	30	250	300 < x ≤ 500	95.33	82.41
18	0.04	15	200	300 < x ≤ 500	88.33	81.72
19	0.06	15	250	300 < x ≤ 500	92.38	83.24
20	0.02	60	200	300 < x ≤ 500	92.54	82.03
21	0.04	30	150	300 < x ≤ 500	90.71	90.54
22	0.04	60	250	300 < x ≤ 500	97.23	82.26
23	0.06	30	200	300 < x ≤ 500	91.98	80.83
24	0.06	60	150	300 < x ≤ 500	93.33	92.03
25	0.04	30	200	300 < x ≤ 500	91.83	83.42
26	0.04	30	200	300 < x ≤ 500	92.18	82.99
27	0.06	15	150	300 < x ≤ 500	86.02	86.34
28	0.06	30	250	300 < x ≤ 500	95.11	90.68
29	0.02	15	200	300 < x ≤ 500	87.07	84.71
30	0.04	15	250	300 < x ≤ 500	93.24	90.51

Generally, in terms of adsorbent particle size (D), the outcome showed that MBAC of ≤ 45 μm is more favourable in reducing turbidity, whereas with CAC, a particle size greater than 300 μm was better for the removal of turbidity. The highest turbidity removal efficiency (98.51%) by MBAC was seen in run 9, with 0.06 g (≤ 45 μm in size) agitated for 150 rpm for 60 min. The highest reading for CAC (92.03%) was observed at identical conditions differing only in terms particle size (300 < x ≤ 500 μm). This indicated good adsorption and efficiency of the separation process. Despite their smaller size, MBAC particles were separated completely during the turbidity test without contaminating recovered water samples. The adsorption results of MBAC in this study was similar to Kim et al., [36] findings, whom used iron oxide nanoparticles-impregnated powder activated carbon (IPAC) to remove organic matter from raw water, with removal efficiency of more than 80%. Therefore, the results indicate that the presence of iron oxide impregnated adsorbent material expands adsorption efficiency. Impregnation delivers improved physical and chemical properties of activated carbon, and biochar. As composites, new adsorption sites are formed.

Although surface area may be lower when compared to CAC, iron oxide impregnated composites can display more surface functionalities that enhance adsorption capacity, with broader affinity towards mixed waste and diverse contaminant types.

Modelling turbidity reduction by MBAC and CAC. Screening of the design based on the block analysis of second-order model in the form of analysis of variance (ANOVA) was generated through Design Expert v.11 and presented in Table 4.

Table 4. Sequential model of sum of squares for MBAC and CAC

Adsorbent type	Source	Sum of Squares	df	Mean Square	F-value	p-value
MBAC	Mean vs Total	5.385E+005	1	5.385E+005		
	Block vs Mean	3.19	2	1.59		
	Linear vs Block	484.88	4	121.22	52.89	< 0.0001
	2FI vs Linear	71	6	11.83	10.76	< 0.0001
	Quadratic vs 2FI	46.87	3	15.62	119.34	< 0.0001
	Cubic vs Quadratic	3.03	13	0.23	2.61	0.0135
	Residual	2.86	32	0.089		
	Total	5.391E+005	61	8837.14		
CAC	Mean vs Total	3.98E+05	1	3.98E+05		
	Block vs Mean	179.3	2	89.65		
	Linear vs Block	415.06	4	103.76	3.68	0.0104
	2FI vs Linear	701.16	6	116.86	7.01	< 0.0001
	Quadratic vs 2FI	749.61	3	249.87	626.26	< 0.0001
	Cubic vs Quadratic	6.85	13	0.5272	1.54	0.1619
	Residual	10.3	30	0.3434		
	Total	4.00E+05	59	6785.01		

The significant models were identified by those having p-values less than 0.05. The magnitude of the F-value was then compared to select the best fit model. The largest F-value for MBAC and CAC were 119.34 and 626.26, respectively. Both corresponded to the quadratic model. The larger the F-value, and the smaller the p-value, the more significant are the corresponding coefficient and model terms [36].

Statistical analysis. The aim was to evaluate through experimental design, the model parameters, and to develop a suitable quantitative model based on the obtained responses (Eq. 5).

$$y = \beta_0 + \sum_{i=1}^{k} \beta ijxi + \sum_{i=1}^{k} \beta ijx^2 i + \sum \sum_{i<j=2}^{k} \beta ijxixj + \varepsilon \quad (5)$$

The equation consisted of predicted response (y), the number of factors (k), constant (β_0), i^{th} linear coefficient (β_i), i^{th} quadratic coefficient (β_{ij}), i^{th} interaction coefficient (β_{ij}), the independent variables (x_i), and error (ε). The measured response was in terms of turbidity removal (%) efficiency. An empirical model was generated after deducing the responses of each combination.

The calculation, fitting of values and checking the adequacy of the model, were carried out. The analysis of variance (ANOVA) was tabulated for each factor by using Design Expert ver. 11. An optimization on the parameters for verification process was conducted to test the reliability of the generated empirical model. The lack-of-fit test (Table 5) was performed to compare the residual and pure error of experimental model fit.

Table 5. Lack of fit test for MBAC and CAC

Adsorbent	Source	Sum of Squares	df	Mean Square	F-value	p-value
MBAC	Linear	122.87	46	2.67	24.07	< 0.0001
	2FI	51.88	40	1.30	11.68	0.0005
	Quadratic	5	37	0.14	1.22	0.4106
	Cubic	1.97	24	0.082	0.74	0.7329
	Pure Error	0.89	8	0.11		
CAC	Linear	1464.14	44	33.28	70.38	< 0.0001
	2FI	762.98	38	20.08	42.47	< 0.0001
	Quadratic	13.37	35	0.3821	0.8082	0.6929
	Cubic	6.52	22	0.2964	0.6268	0.8168
	Pure Error	3.78	8	0.4728		

The lack of fit F-value (F_0) for the obtained quadratic model of both MBAC and CAC were 1.22 and 0.8082, respectively. The p-values, 0.4106 for MBAC and 0.6929 for CAC were also relatively large. These results imply that a lack of fit for these models is not significant relative to the pure error [28]. The lack of fit term is insignificant, we accept the hypothesis that the quadratic models are valid and adequately describe the current experimental turbidity reduction process.

Model Adequacy. Assessing the adequacy of the model is critical to ensure that the empirical models have an adequate approximation to the true process and to verify that the assumptions for square regression are at the point of view [39]. An adequate empirical model must fulfil three residual assumptions, consisting of a normal distribution, constant variance, and independence [38]. Fig. 4 (i) shows the normal probability and residual plots for both MBAC and CAC. Majority of the points are concentrated along the central portion of the data, and these observations verify that the residuals are normal.

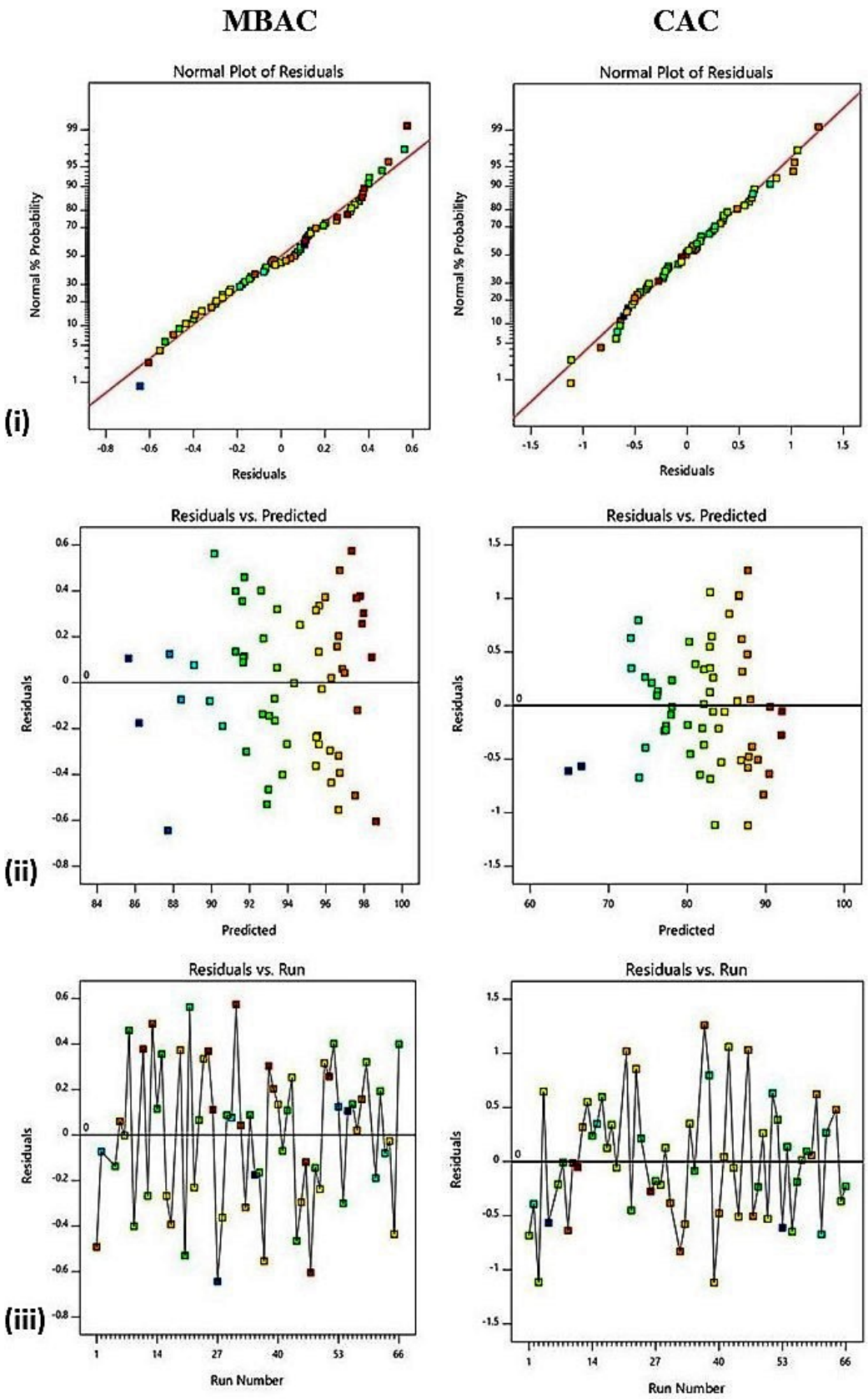

Fig. 4. Model adequacy for turbidity removal process efficiency by MBAC and CAC described through (i) residual and normal probability plots, (ii) predicted and residual plots, and (iii) residual plots by run numbers

As there are no unusually large residuals, hence, a transformation of the response is not required, as stated by Kumar et al.,[38]. Moreover, it can be seen in Fig. 4 (ii) that the residuals are scattered randomly with homoscedasticity. The results reveal that the variance of residuals is constant for all

values of Y [39]. Another criterion in expressing the adequacy of the model is the assumption of the independent residual. The assumption will be violated if there is a dependence between residuals which can be observed upon negative or positive pattern of residual plots against time. Based on Fig. 4 (iii), there are no discernible pattern of graphs for both MBAC and CAC hence the residuals are deemed to be independent [40].

Analysis of variance (ANOVA) of turbidity reduction study. Table 6 lists the analysis of variance (ANOVA) relating to the correlation between process variables and processing parameters.

Table 6. Analysis of variance (ANOVA) for turbidity removal efficiency by MBAC and CAC. The coded variables denote A: adsorbent dosage, B: agitation time, C: agitation rate, and D: particle size range of adsorbent

Adsorbent	Source	Sum of Squares	DF	Mean Square	F-Value	Prob > F
MBAC	Block	3.19	2	1.59		
	Model	602.75	13	46.37	354.14	< 0.0001
	A	0.97	1	0.97	7.39	0.0093
	B	114.13	1	114.13	871.72	< 0.0001
	C	75.09	1	75.09	573.55	< 0.0001
	D	297.96	1	297.96	2275.79	< 0.0001
	A^2	1.97	1	1.97	15.06	0.0003
	B^2	31.34	1	31.34	239.37	< 0.0001
	C^2	22.75	1	22.75	173.75	< 0.0001
	AB	0.17	1	0.17	1.32	0.2572
	AC	1.94	1	1.94	14.85	0.0004
	AD	8.13	1	8.13	62.08	< 0.0001
	BC	27.37	1	27.37	209.05	< 0.0001
	BD	16.25	1	16.25	124.09	< 0.0001
	CD	26.25	1	26.25	200.47	< 0.0001
	Residual	5.89	45	0.13		
	Lack of Fit	5	37	0.14	1.22	0.4106
	Pure Error	0.89	8	0.11		
	Cor Total	611.83	60			
CAC	Block	179.3	2	89.65		
	Model	1865.82	13	143.52	359.72	< 0.0001
	A	168.57	1	168.57	422.48	< 0.0001
	B	2.11	1	2.11	5.28	0.0264
	C	46.77	1	46.77	117.21	< 0.0001
	D	177.41	1	177.41	444.65	< 0.0001
	A^2	219.16	1	219.16	549.29	< 0.0001
	B^2	62.6	1	62.6	156.89	< 0.0001
	C^2	622.53	1	622.53	1560.28	< 0.0001
	AB	757.16	1	757.16	1897.71	< 0.0001
	AC	1.16	1	1.16	2.91	0.095
	AD	49.03	1	49.03	122.88	< 0.0001
	BC	32.36	1	32.36	81.11	< 0.0001
	BD	98.75	1	98.75	247.51	< 0.0001
	CD	5.26	1	5.26	13.18	0.0007
	Residual	17.16	43	0.4		
	Lack of Fit	13.37	35	0.38	0.81	0.6929
	Pure Error	3.78	8	0.47		
	Cor Total	2062.28	58			

The coded variables denote A: adsorbent dosage, B: agitation time, C: agitation rate, and D: particle size range of adsorbent

The analysis was tagged at 95% confidence interval covering the model parameters. Model terms are accepted as significant if the value of Prob > F was less than 0.05. From the table it was decided that the process model was significant ($p < 0.0001$) for both adsorbents with model F-values of 354.14 for MBAC and 359.72 for CAC.

The non-significant terms for MBAC (AB; p-value > 0.05) and CAC (AC; p-value > 0.05) were identified and dropped from the empirical model generation. It is important to drop the non-significant terms as there are differences between full and reduced model in predicted error sum of squares (PRESS) and Adjusted R-Squared (Table 7).

Table 7. Comparison between full quadratic and reduced quadratic model for turbidity removal efficiency between MBAC and CAC

Adsorbent Source	MBAC		CAC	
	Full quadratic model	Reduced quadratic model	Full quadratic model	Reduced quadratic model
Std. Dev	0.36	0.36	0.63	0.65
Mean	93.95	93.95	82.16	82.16
CV	0.39	0.39	0.77	0.79
PRESS	11.68	11.32	34.46	35.35
R^2	0.9903	0.9900	0.9909	0.9903
Adjusted R^2	0.9875	0.9874	0.9881	0.9876
Predicted R^2	0.9808	0.9814	0.9817	0.9812
Adequate Precision	70.049	72.204	82.74	84.349

The analysis supported well the generated empirical models as more than half of the terms in ANOVA are significant. Shahmoradi [36] also suggested that the representation of the generated empirical model is better satisfied after dropping non-significant terms. For both adsorbents, the quadratic model produced excellent correlation as seen from R^2 (~0.99), adjusted R^2 (~0.98), and predicted R^2 (~0.98) values. The relatively high R^2 readings with both adsorbents reflected good agreements between experimental and predicted values. The quadratic model can be used to navigate the process design space for both adsorbents.

Empirical model development for turbidity reduction study. An empirical mathematical model had been generated through the method of steepest ascent and multiple regression analysis of experimental data (Table 3). The predicted response (Y%) for turbidity removal by MBAC (Y_{MBC}, Eq. 6) and CAC (Y_{CAC}, Eq. 7) were expressed based upon second-order polynomial (quadratic) equation. The model was used to describe the correlation between the investigated variables and turbidity removal %. In the model's equation, A B, C, and D, are coded variables for adsorbent dosage, agitation time, agitation rate, and particle size range of adsorbent, respectively. The estimated response at the stationary point (centre of the system) for MBAC is 94.87, and 82.03 for CAC. Therefore, it is assumed that the performance of MBAC in removing turbidity in raw groundwater is greater than CAC. The negative signs in the equations indicate antagonistic effect; meanwhile, the positive signs indicate synergistic effect. As the generated empirical equations (Eq. 6 and Eq. 7) are mixed in positive and negative signs, reflecting that the stationary point is a saddle point [40]. So, the strategy for improving turbidity removal efficiency in the saddle system is flexible (i.e., minimum and maximum range of each variable are considered in optimization process) and depends on the nature of the response system.

$$Y_{MBC}\ (\%) = 94.87 - 0.17A + 1.85B + 1.59C + 2.28D - 0.39A^2 - 1.82B^2 + 1.33C^2 - 0.31AC - 0.5AD - 1.11BC - 0.68BD - 0.94CD \quad (6)$$

$$Y_{CAC}\ (\%) = 82.03 + 2.36A - 0.27B - 1.26C + 1.80D - 4.29A^2 - 2.62B^2 + 7.27\ C^2 + 5.88AB + 1.26AD - 1.25BC - 1.82BD + 0.42CD \quad (7)$$

Effect of adsorption process parameters. The perturbation plot was used to investigate changes in response (turbidity removal %) as each individual factors, i.e., adsorbent dosage (A), agitation time (B), agitation rate (C), and particle size range of adsorbent (D) was removed from the selected reference point while the other factors at the reference point were held constant. The reference point is the coded zero level in the middle of the design space. A steep slope in the result suggests the sensitivity of response to a factor. As far as the slope was concerned, positive coefficient is pushed up while negative coefficient is pressed down [41]. The perturbation plots for MBAC and CAC over the two adsorbent particle size ranges, ≤ 45 μm and 300 < x ≤ 500 μm are given in Fig. 5. The plot of MBAC as in Fig. 5 (a) depicts factor A (adsorbent dosage) as relatively a flat line. This indicates that turbidity removal efficiency is insensitive towards changes in dosage of adsorbent (A). Meanwhile the steepest curve of factor B (agitation time) and C (agitation rate) indicate that turbidity removal efficient is sensitive to agitation time and rate. Turbidity removal efficiency over varying dosage of MBAC (0.02, 0.04, and 0.06 g) showed relatively small difference. This might be due to the presence of iron oxide particles that improves surface and pore driven adsorptions. Besides, magnetic separation of MBAC ensures cleaner groundwater without any traces of residual adsorbent regardless of the amount of dosage used.

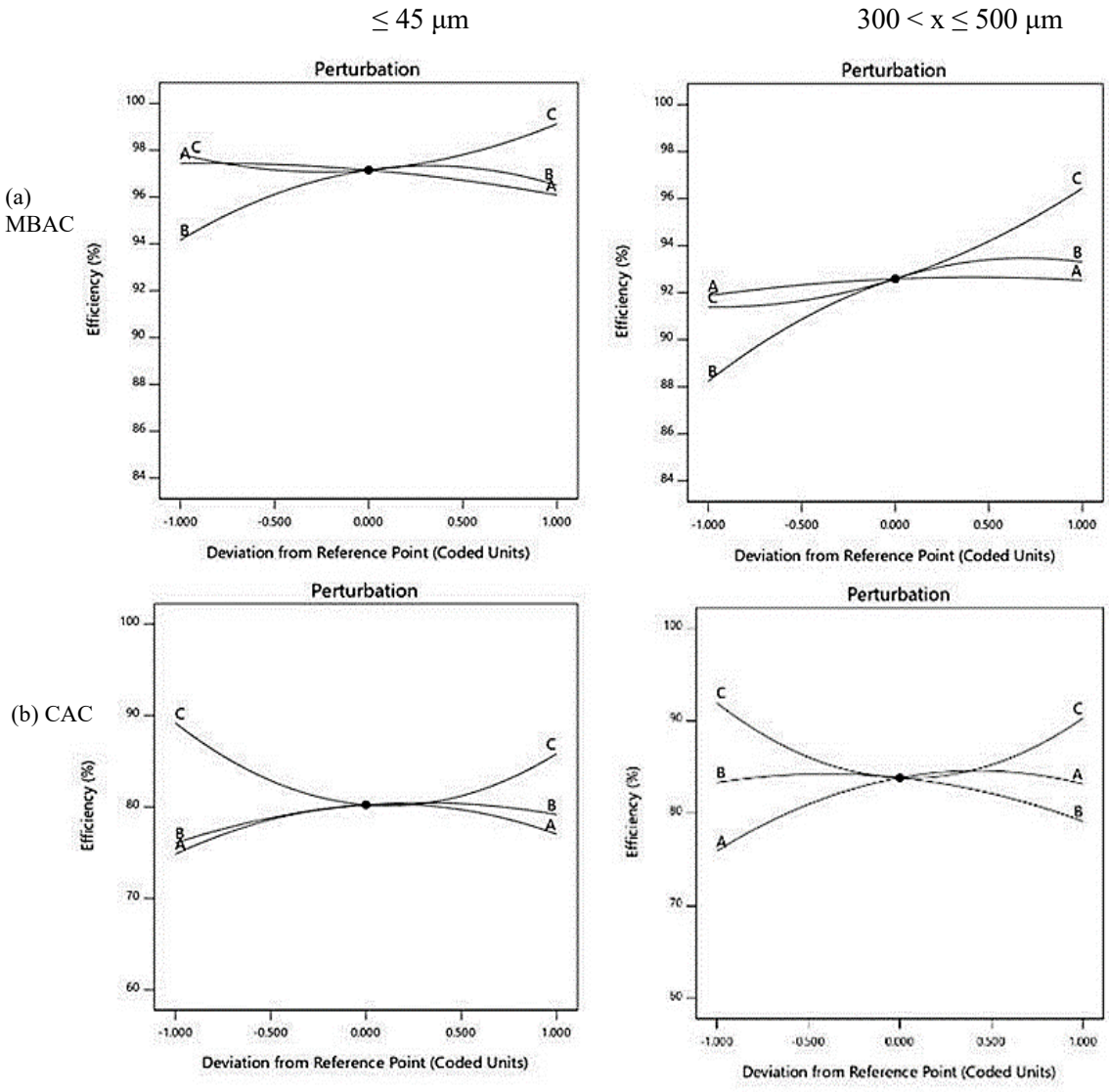

Fig. 5. Perturbation plots describing turbidity removal efficiency differentiated by particle size range of ≤ 45 μm and 300 < x ≤ 500 μm for (a) MBAC and (b) CAC

When comparing to perturbation plots of CAC with the size of adsorbent ≤ 45 μm and 300 < x ≤ 500 μm in Fig. 5 (b), factor B (agitation time) showed relatively smaller effect as it moved from the reference point. Factor C (agitation rate) showed steepest curve in at both particle size ranges. Hence, it indicated that turbidity removal is insensitive to agitation time (B) but sensitive to agitation rate (C). The effect of factor A (dosage of adsorbent) is dynamic between the two ranges of adsorbent size. Turbidity removal efficiency is more sensitive to adsorbent dosage of larger size (300 < x ≤ 500 μm). Rapid adsorption might be the reason as to why turbidity removal efficiency is relatively indifferent towards agitation time. On the other hand, separation efficiency was somewhat weaker with CAC. Since CAC did not display magnetic properties, separation of spent CAC was done by filtration which might had left some adsorbent residues in the groundwater sample. This may affect water treatment initiative at the point of use in the future as separation of spent material needs to be addressed.

Process optimization for turbidity reduction by MBAC and CAC. The interaction between the variables and their optimum levels can be depicted through 3D response surface and 2D contour plots. The significance of interaction is displayed by elliptical shape, whereas circular shape indicates insignificant interaction. Fig. 6 (a) shows the interaction between agitation rate (C) and adsorbent dosage (A) for MBAC. The increase in adsorbent dosage from 0.02 g to 0.04 g improved turbidity removal efficiency %. The decline in turbidity removal efficiency occurred when adsorbent dosage is over 0.04 g, and there is no obvious effect when agitation rate is beyond 150 rpm. The turbidity removal efficiency decreases at a relatively high agitation rate as target pollutants in raw turbid groundwater and adsorbent are hastily colliding with each other and may lead to detachment of loosely bound impurities [42]. Plot in Fig. 6 (b) shows that the optimum turbidity removal % by MBAC by time lies between 24 to 33 min. The increment in agitation time may improve turbidity removal efficiency, but it does not show the obvious effect as agitation rate increased. The rapid adsorption may occur due to diffusion control from the bulk of the liquid phase to the unoccupied binding site at the surface of adsorbent [42]. A study by Liang et al., [43] commented that rapid adsorption of contaminants occurs at the initial phase, over the occupied sites of $CoFe_2O_4$/AC, and adsorption decreases at the later stage.

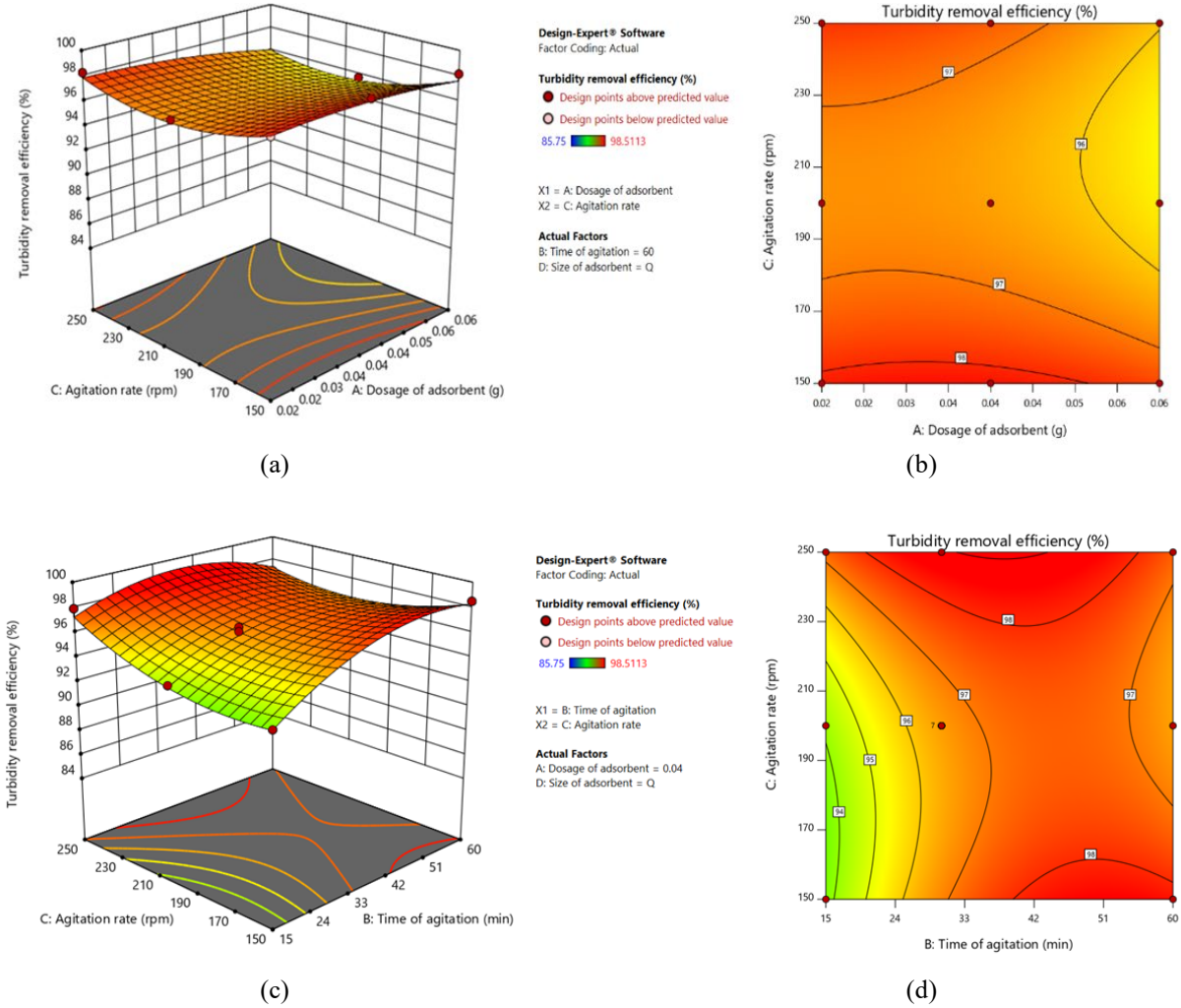

Fig. 6. Response surface and contour plot of MBAC for turbidity removal efficiency as a function of (a) adsorbent dosage and agitation rate (AC), (b) agitation time and agitation rate (BC)

Fig. 7 (a) exhibits the relationship between adsorbent dosage and agitation time (AB) on turbidity removal efficiency. The increase in adsorbent dosage along with time improved turbidity removal efficiency. However, the removal efficiency declined as adsorbent dosage exceeded 0.04 g, and agitation time was beyond the 24 to 33 min range. Slower paced adsorption may occur at a later stage with any of the remaining adsorption sites.

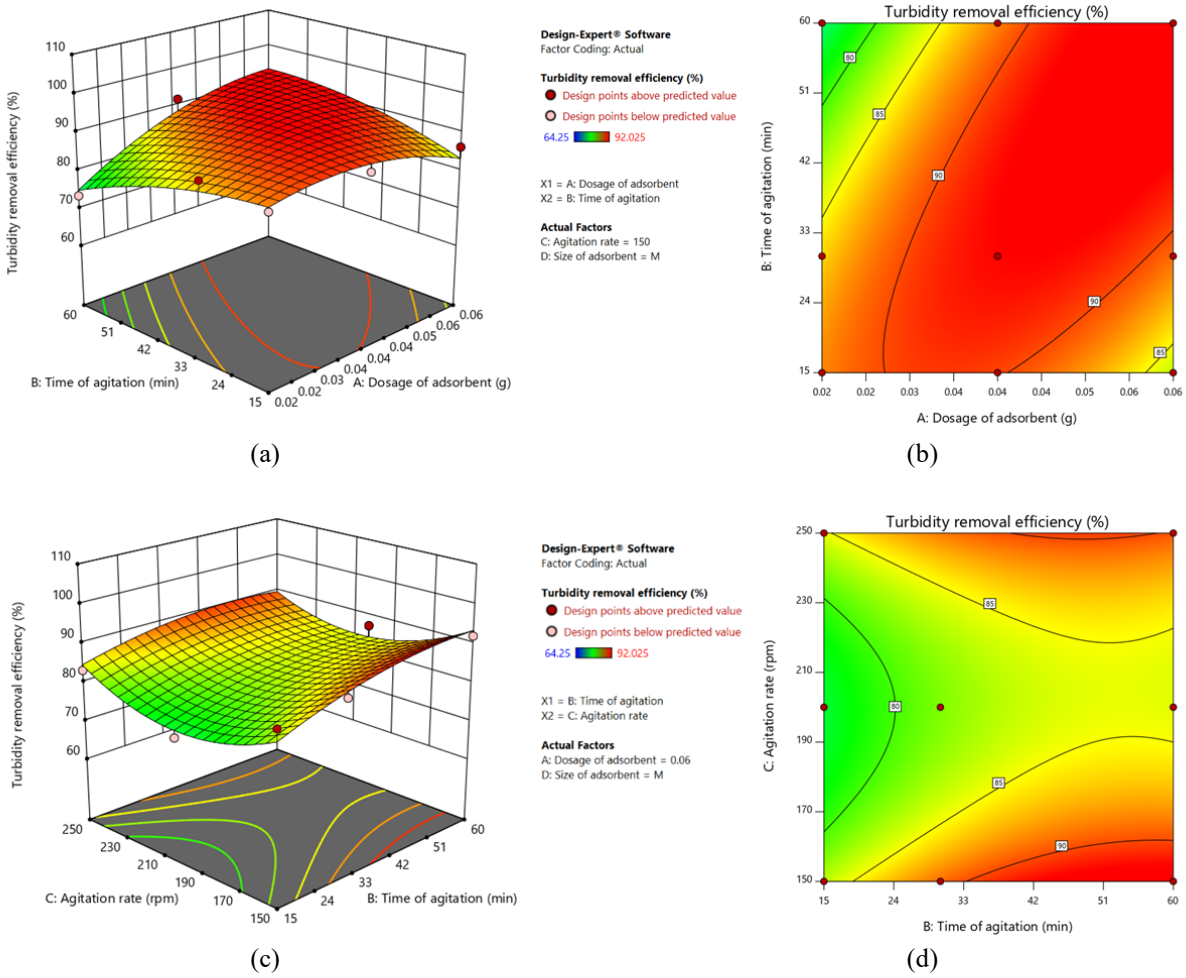

Fig. 7. Response surface and contour plot of CAC for turbidity removal efficiency as a function of (a) adsorbent dosage and agitation time (AB), (b) agitation time and agitation rate (BC)

Furthermore, the interaction between time of agitation and agitation rate in Fig. 7 (b) portrays that optimum turbidity removal efficiency lies in the range of 24 to 33 min, and 190 to 210 rpm. Turbid solute that reduces the surface tension of water is easily taken up and adsorbed by CAC. Higher rate of collision results in higher adsorption. However, physical adsorption involves weak van der Walls force [44]. So, it is unlikely to affect final turbidity removal efficiency during the later stage at agitation rate of above 210 rpm.

Basically, adsorption can be viewed as a 3-step process [45]. In the first step, adsorbates diffuse into the fluid film and attach onto the adsorbent surface. Then, the attached absorbate migrate from the external surface area into the pores of the adsorbent through diffusion (step 2). This step is also known as mixed diffusion due to the occurrence of two processes at the same time, i.e., pore diffusion and surface diffusion. The continuous adsorption processes in the pore sites ensue in step 3. Two mechanisms have been postulated regarding to adsorption onto iron oxide surfaces [11]. The first would be by van der Waals interactions with the oxide surface (physisorption) or chemical reactions with the functional groups (chemisorption). The second mechanism is through ion exchange of pollutant ions in aqueous solution with iron ions in the iron oxide lattice structure.

Verification of the predictive model. The optimization experiment was conducted to verify the identified optimum conditions with the highest desirable output as generated by Design Expert v.11 software for turbidity removal efficiency (%). Table 8 shows the prescribed optimum condition and actual results obtained with MBAC and CAC.

Table 8. Predicted and actual turbidity removal efficiency (%) values at optimized parameters for MBAC and CAC

Adsorbent	Adsorbent dosage (g)	Agitation time (min)	Agitation rate (rpm)	Adsorbent particle size range (µm)	Condition	Turbidity removal efficiency (%)
MBAC	0.04	48	150	≤ 45	Predicted	98.50
					Actual	98.46
CAC	0.05	45	150	300 < x ≤ 500	Predicted	92.46
					Actual	88.19

Treatment with MBAC achieved a turbidity removal efficiency of 98.46% (final NTU reading of 0.40), close to the predicted value of 98.50%. Turbidity removal with CAC was 88.19% (final NTU reading of 3.07), about 4% below the predicted 92.46%. Initial NTU reading of the groundwater was 26 NTU. Indeed, the raw groundwater treated with either MBAC and CAC complied to the National Drinking Water Quality Standard [7], where acceptable turbidity reading is set at below 5 NTU. The results revealed that the optimization parameters were reliable with no significant difference between predicted and actual results. Hence, all models are valid. Fig. 8 shows the groundwater appearance after subjected to treatment with MBAC.

Fig. 8. Appearance of the raw groundwater. (a) before treatment (26 NTU) and (b) after treatment with MBAC (0.4 NTU)

For further exploring of MBAC's usefulness, the raw groundwater (tagged as sample A) and the groundwater treated with MBAC (tagged as sample B) were outsourced for laboratory analyses (Acumen Scientific Sdn. Bhd., Accredited Laboratory, Standards Malaysia MS ISO/IEC 17025, Testing SAMM No. 541). The test results are presented in Table 9. The raw groundwater exhibited high levels of Al (13.21 mg/L), Fe (14.97 mg/L), Mn (0.5 mg/L), and Pb (0.03 mg/L) which exceeded the Malaysia Food Act 1983 & Regulation 1985 set limits. The source of groundwater collected either from well or tube well in the districts of Tanah Merah are known to harbour high concentrations of Fe and Mn, with turbidity up to 39.10 NTU, and acidic (pH ~ 5) in nature [47]. Following treatment with MBAC, Al, Fe, and Mn levels decreased over 80% to 2.34 mg/L, 2.61 mg/L, and 0.1 mg/L, respectively. Pb was not detected (< 0.01 mg/L) after treatment. Similarly, lower amount of Ba, Ca, Cu, Mg, P, Zn, total chlorine, suspended solids, and total dissolved solids were observed in sample B which underwent treatment with MBAC compared to sample A (raw groundwater).

Table 9. Laboratory analysis of raw groundwater (sample A) and after subjected to MBAC treatment (sample B) ND: not detected (< numeric number) denotes detection limits. Remark: Specification limits based on 25th A Schedule, Drinking Water Standards [6, 7, 46].

Parameter, unit	Sample A (before); Certificate no: CCA19030771W01-0	Sample B (after); Certificate no: CCA19030772W01-0	Limits	Standard method / technique
Conductivity, µs/cm	61.3	58.5	-	APHA 2510 B (2012)
Salinity, PSU	0.035	0.034	-	APHA 2520 B (2005)
pH	7.1	6.7	6.5-8.5	APHA 4500-H+ B (2005)
Total organic carbon (TOC), mg/L	870	1000	-	APHA 5310-C
Suspended solids, mg/L	162	14	-	APHA 2540 D (2005)
Total dissolved solids, mg/L	179	112	-	APHA 2540C (2005)
Aluminium, mg/L	13.21	2.34	0.2	APHA 3120 B (2005)
Ammoniacal nitrogen, mg/L	0.42	0.44	-	APHA 4500-NH3 F (2005)
Antimony, mg/L	ND (<0.005)	ND (<0.005)	0.005	APHA 3120 B (2005)
Arsenic, mg/L	ND (<0.005)	ND (<0.005)	0.01	APHA 3030 F & 3120 B (2005)
Barium, mg/L	0.09	0.03	0.7	APHA 3030 F & 3120 B (2005)
BOD_5, mg/L	5	3	-	APHA 5210 B (2005)
COD, mg/L	15	10	-	APHA 5220 D (2005)
Boron, mg/L	ND (<0.01)	ND (<0.01)	0.5	APHA 3030 F & 3120 B (2005)
Cadmium, mg/L	ND (<0.005)	ND (<0.005)	0.003	APHA 3030 F & 3120 B (2005)
Calcium, mg/L	7.94	3.76	-	APHA 3120 B (2005)
Chromium, mg/L	0.02	ND (<0.005)	0.05	APHA 3030 F & 3120 B (2005)
Copper, mg/L	0.14	0.03	1	APHA 3030 F & 3120 B (2005)
Coliform [MPN], MPN/100 mL	4.5	23	<10	APHA 9221 B (MPN) (2005)
E. coli [MPN], MPN/100 mL	ND (<1.8)	ND (<1.8)	Absent	APHA 9221 B (MPN)
Heterotrophic plate count [Pour Plate], CFU/mL	1.4×10^5	6.2×10^4	-	APHA 9215B (Pour Plate Method)
Iron, mg/L	14.97	2.61	0.3	APHA 3030 F & 3120 B (2005)
Lead, mg/L	0.03	ND (<0.01)	0.01	APHA 3030 F & 3120 B (2005)
Magnesium, mg/L	2.01	1.06	150	APHA 3120 B (2005)
Manganese, mg/L	0.50	0.10	0.1	APHA 3030 F & 3120 B (2005)
Mercury, mg/L	ND (<0.005)	ND (<0.005)	0.001	APHA 3112 B (2005)
Phosphorus, mg/L	0.4	0.3	-	APHA 4500-P C (2005)
Selenium, mg/L	ND (<0.005)	ND (<0.005)	0.01	APHA 3030 F & 3120 B (2005)
Silver, mg/L	ND (<0.01)	ND (<0.01)	0.05	APHA 3030 F & 3120 B (2005)
Sodium, mg/L	3.87	3.85	200	APHA 3120 B (2005)
Total chlorine, mg/L	0.08	0.03	-	APHA 4500-Cl (2005)
Zinc, mg/L	0.24	0.03	3	APHA 3030 F & 3120 B (2005)

ND: not detected (< numeric number) denotes detection limits. Remark: Specification limits based on 25th Schedule (A), Standard for Water, Malaysia Food Act 1983 & Regulation 1985.

A review by Ahmed et al., [48] have noted that magnetic biochars remove higher % of water pollutants such as As, Pb, and Cd from water due to the fact that γ-Fe_2O_3 nanoparticles can also serve as sorption sites through electrostatic interactions. The potential combination of targeted adsorption-based processes with MBAC and existing water treatment methods can be further explored. The proposed mechanism of action is presented in Fig. 9. The alternative approach may prove to be more technically and economically feasible.

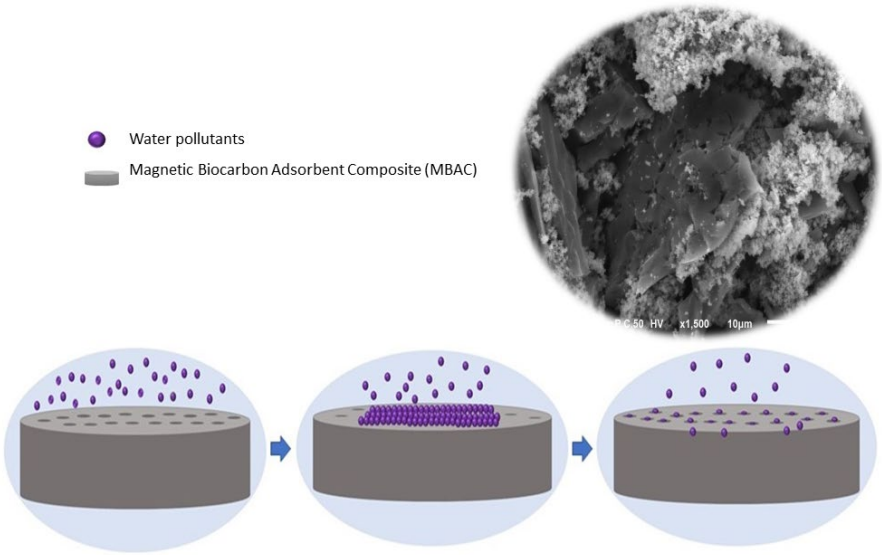

Fig. 9. Proposed mechanism governing combined turbidity and water pollutants adsorption and removal by MBAC

Conclusion

The successful preparation and testing of a newly synthesized magnetic biocarbon adsorbent composite (MBAC) for the reduction of turbidity in groundwater had been demonstrated. Process optimization was performed by comparing adsorption properties to a commercial activated carbon (CAC). The RSM approach was adopted in the study to optimize turbidity removal efficiency. Model adequacy analysis revealed that the generated quadratic model best fitted the experimental output. The adsorbent dosage (A) and agitation time (B) were found to be the least important factor for MBAC and CAC from the quadratic model developed for turbidity removal efficiency and variance analysis (ANOVA). The findings showed the advantageous role of iron oxide in the biocarbon adsorbent composite for turbidity reduction. The optimum process parameters for MBAC were to apply 0.04 g of adsorbent that is ≤ 45 μm in size, agitated at 150 rpm for 48 min. The models were accurate and validated for both adsorbents accordingly. Both adsorbents were beneficial for reducing the level of turbidity from 26 NTU to less than 5 NTU. However, MBAC displayed better removal efficiency (98.46%) by 10% compared to CAC. Furthermore, spent MBAC can be easily separated from water by applying external magnetic force, and eliminates the need for filtration and sedimentation. The obtained empirical model can be used as reference for scaling up, and devising a working filter or active filtration unit for point of use.

Acknowledgement

This study was financially supported by Universiti Malaysia Kelantan Grants (R/SGJP/A07.00/01397A/005/2018/00570 & R/PRO/A07.00/01397A/008/2021/00975). We also like to thank our industry collaborators, Mr. Abda Jamil from AJ Sinari Ventures & SIRIM Bhd.

References

[1] Information on https://www.sinarharian.com.my/article/990/EDISI/Kelantan/AKSB-diiktiraf-Malaysia-Book-of-Records

[2] SPAN (Suruhanjaya Perkhidmatan Air Negara), Annual Report, (2018) 30.

[3] F.R. Mohd Faiz, M. Noorazuan, Perubahan kualiti air bawah tanah di negeri Kelantan pada tahun 2010 hingga 2012, JWS. 2 (2018) 1-10.

[4] H.H. Hazimah, M.K. Mohamad Roslan, S. Nurhidayu, A. Zulfa Hanan, M.K. Faradiella, Hydrogeochemistry investigation on groundwater in Kuala Langat, Banting, Selangor, Bull. Geol. Soc. Malays. 67 (2019) 127-134.

[5] R. Muoio, C. Caretti, L. Rossi, D. Santianni, C. Lubello, Water safety plans and risk assessment: A novel procedure applied to treated water turbidity and gastrointestinal diseases C, Int J Hyg Environ Health. 223 (2020) 281-288.

[6] Information on https://www.who.int/water_sanitation_health/hygiene/emergencies/fs2_33.pdf

[7] Information on http://kmam.moh.gov.my/public-user/drinking-water-quality-standard.html

[8] G.S. Simate, S.E. Iyuke, S. Ndlovu, M. Heydenrych, L.F. Walubita, Human health effects of residual carbon nanotubes and traditional water treatment chemicals in drinking water, Environ. Int. 39 (2012) 38-49.

[9] M. Karnib, A. Kabbani, H. Holail, Z. Olama, Heavy metals removal using activated carbon, silica and silica activated carbon composite, Energy Procedia. 50 (2014) 113-120.

[10] P. Meng, X. Fang, A. Maimaiti, G. Yu, S. Deng, Efficient removal of perfluorinated compounds from water using a regenerable magnetic activated carbon, Chemosphere. 224 (2019) 187-194.

[11] D. Dermatas, T. Mpouras, N. Papassiopi, C. Mystrioti, A. Toli, I. Panagiotakis, Adsorption of groundwater pollutants by iron nanomaterials, in: M.I. Litter, N. Quici, M. Meichtry (Eds), Iron nanomaterials for water and soil treatment, Pan Stanford Publishing Pte. Ltd., Singapore, 2018 pp. 37-55.

[12] C. Santhosh, A. Malathi, E. Dhaneshvar, A. Bhatnagar, A.N. Grace, J. Madhavan, Nanoscale materials in water purification, Elsevier Inc, Amsterdam, Netherlands. 2019.

[13] P. Tancredi, L.S. Veiga, O. Garate, G. Ybarra, Magnetophoretic mobility of iron oxide nanoparticles stabilized by small carboxylate ligands, Colloids Surf. A. 579 (2019) 123664.

[14] A.L. Cazetta, O. Pezoti, K.C. Bedin, T.L. Silva, A. Paesano Junior, T. Asefa, V.C. Almeida, Magnetic activated carbon derived from biomass waste by concurrent synthesis: efficient adsorbent for toxic dyes, ACS Sustain Chem Eng. 4 (2016) 1058-1068.

[15] W. Park, S. Jeong, S. Im, A. Jang, High turbidity water treatment by ceramic microfiltration membrane: Fouling identification and process optimization, Environ. Technol. Innov. 17 (2020) 100578.

[16] P. Sannasi, A. Huda, B. Jayanthi, Synthesis of magnetic activated carbon treated with sodium dodecyl sulphate, Pertanika J. Sci. Technol. 29 (2021) 427-444.

[17] A. Nor Asfaliza, P. Sannasi, M.A. Mohamad Faiz, Modifying coconut shell biocarbon by base activation method using response surface modelling, ARPN J. Eng. Appl. Sci. 16 (2020) 1778-1783.

[18] R. Wannahari, P. Sannasi, M.F.M. Nordin, H. Mukhtar, Sugarcane bagasse derived nano magnetic adsorbent composite (SCB-NMAC) for removal of Cu^{2+} from aqueous solution, ARPN J. Eng. Appl. Sci. 13 (2018) 1-9.

[19] Information on http://osmindustrial.com/wp-content/uploads/2017/10/ASTM-D4607-Standard-Test-Method-for-Determination-of-Iodine-Number-of-Activated-Carbon.pdf

[20] A. Mianowski, M. Owczarek, A. Marecka, Surface area of activated carbon determined by the iodine adsorption number, Energy Sources. 29 (2007) 839-850.

[21] C.A. Nunes, M.C. Guerreiro, Estimation of surface area and pore volume of activated carbons by methylene blue and iodine numbers, Quim Nova. 34 (2011) 472-476.

[22] T.A. Milne, H.L. Chum, F.A. Agblevor, D.K. Johnson, Standardized analytical methods biomass & bioenergy, Proceedings of International Energy Agency Bioenergy Agreement Seminar. 2 (1992) 341-366.

[23] K.W.N. Wan Fatihah, C.S. Siti Kamila, A.R.A. Alyza Azzura, M.Y. Mohd Sukeri, S. Mustaffa, Synthesis and physicochemical properties of magnetite nanoparticles (Fe_3O_4) as potential solid support for homogeneous catalysts, Malays. J. Anal. Sci. 22 (2018) 768-774.

[24] S. Karthikeyan, P. Sivakumar, P.N. Palanisamy, Novel activated carbons from agricultural wastes and their characterization, E-J. Chem. 5 (2008) 409-426.

[25] A.F.G.H. Zulkarnia, A.S. Rezki, The potential of activated carbon derived from bio-char waste of bio-oil pyrolysis as adsorbent, MATEC Web of Conference. 01029 (2018) 1-6.

[26] X. Zhao, S. Yi, S. Dong, H. Xu, Y. Sun, X. Hu, Removal of Levofloxacin from aqueous solution by magnesium-impregnated biochar: Batch and column experiments, Chem. Speciat. Bioavailab. 30 (2018) 68-75.

[27] A.R. Hidayu, N.F. Mohamad, S. Matali, A.S.A.K. Sharifah, Characterization of activated carbon prepared from oil palm empty fruit bunch using BET and FT-IR techniques, Procedia Eng. 68 (2013) 379-384.

[28] S. Mopoung, P. Moonsri, W. Palsa, S. Khumpai, Characterization and properties of activated carbon prepared from tamarind seeds by KOH activation for Fe (III) adsorption from aqueous solution, Sci. World J. 2015 (2015) 415961.

[29] H. Sun, B. Yang, A. Li, Biomass derived porous carbon for efficient capture of carbon dioxide, organic contaminants and volatile iodine with exceptionally high uptake, Chem. Eng. J. 372 (2019) 65–73.

[30] Information on https://chem.libretexts.org/Ancillary_Materials/Reference/Reference_Tables/Spectroscopic_Parameters/Infrared_Spectroscopy_Absorption_Table

[31] Information on https://www2.chemistry.msu.edu/faculty/reusch/virttxtjml/spectrpy/infrared/infrared.htm

[32] A. Mirzaei, K. Janhorban, B. Hashemi, S.R. Hosseini, M. Bonyani, S.G. Leonardi, A. Bonavita, G. Neri, Synthesis and characterization of mesoporous α-Fe_2O_3 nanoparticles and investigation of electrical properties of fabricated thick films, Process. Appl. Ceram. 1 (2016) 209-217.

[33] P. Suresh Kumar, T. Prot, L. Korving, K.J. Keesman, I. Dugulan, M.C.M. van Loosdrecht, G.J. Witkamp, Effect of pore size distribution on iron oxide coated granular activated carbons for phosphate adsorption – Importance of mesopores, Chem. Eng. J. 326 (2017) 231-239.

[34] C. Anyika, N.A.M. Asri, Z.A. Majid, A. Yahya, A. Jaafar, Synthesis and characterization of magnetic activated carbon developed from palm kernel shells, Nanotechnol. Environ. Eng. 2 (2017) 16.

[35] N.D. Kandpal, N. Sah, R. Loshali, R. Joshi, J. Prasad, Co-precipitation method of synthesis and characterization of iron oxide nanoparticles, J. Sci. Ind. Res. 73 (2014) 87-90.

[36] S. Kim, J. Kim, G. Seo, Iron oxide nanoparticle-impregnated powder-activated carbon (IPAC) for NOM removal in MF membrane water treatment system, Desalination Water Treat. 51 (2013) 6392-6400.

[37] B. Shahmoradi, S. Yavari, Y. Zandsalimi, H.P. Shivaraju, M. Negahdari, A. Maleki, G. Mckay, R.P. Radheshyam, S.M. Lee, Optimization of solar degradation efficiency of bio-composting leachate using Nd: ZnO nanoparticles, J. Photochem. Photobiol. A. 356 (2018) 201-211.

[38] S. Kumar, H. Meena, S. Chakraborty, B.C. Meikap, Application of response surface methodology (RSM) for optimization of leaching parameters for ash reduction from low-grade coal, Int. J. Min. Sci. Technol. 28 (2018) 621-629.

[39] A.U.F. Tezcan, N. Erginel, O. Ozcan, E. Oduncu, Adsorption of Disperse Orange 30 dye onto activated carbon derived from Holm Oak (*Quercus Ilex)* acorns: A 3k factorial design and analysis, J. Environ. Manage. 155 (2015) 89-96.

[40] R.H. Myers, D.C. Montgomery, C.M. Anderson-Cook, Response surface methodology, fourth ed., John Wiley & Sons, New Jersey, 2016.

[41] M.J. Anderson, P.J. Whitcomb, RSM Simplified, second ed, CRC Press, London, 2017.

[42] G.K. Latinwo, A.O. Alade, S.E. Agarry, E.O. Dada, Process optimization and modeling the adsorption of polycyclic aromatic-congo red dye onto *Delonix regia* pod-derived activated carbon, Polycycl. Aromat. Compd. 3 (2019) 38-45.

[43] Y. Liang, Y. He, T. Wang, L. Lei, Adsorptive removal of gentian violet from aqueous solution using $CoFe_2O_4$ / activated carbon magnetic composite, J. Water Process. Eng. 27 (2019) 77-88.

[44] H.B.W. Patterson, Bleaching and purifying fats and oils theory and practice, Elsevier Inc, Netherlands, 2009.

[45] F.R. Spellman, N.E. Whiting, Environmental Engineer's Mathematics Handbook, CRC Press LLC, Boca Raton, 2005.

[46] Information on https://www.moh.gov.my/index.php/database_stores/attach_download/317/16

[47] A. Huda, P. Sannasi, A.L. Zul Ariff, A preliminary study of local behaviour, perceptions and willingness to pay towards better water quality in Pasir Mas, Tanah Merah, and Jeli, Malaysia, IOP Conf. Ser. Earth Environ. 549 (2020) 012086.

[48] M.B. Ahmed, J.L. Zhou, H.H. Ngo, W. Guo, M. Chen, Progress in the preparation and application of modified biochar for improved contaminant removal from water and wastewater, Bioresour. Technol. 214 (2016) 836-851.